Optimizing control fields for diabatic protocols in the presence of noise

Marllos E. F. Fernandes ⬛, Emanuel F. de Lima ⬛, and Leonardo K. Castelano ⬛*

Departamento de Física, Universidade Federal de São Carlos, São Carlos, São Paulo 13565-905, Brazil

Quantum control techniques are employed to perform quantum algorithms inspired by the adiabatic quantum computing protocols in the presence of noise. First, we analyze the entanglement protocol for two qubits. In this case, we find that this protocol is very robust against noise. The reason behind this fact is related to the chosen Hamiltonians, where the ground state of the initial Hamiltonian is not affected by the noise. The optimal control solution, in this case, is to leave the system in its ground state and apply a fast pulse to entangle the qubits at the end of the time evolution. Second, we probe a system composed of three qubits, where the goal is to teleport the first qubit to the third qubit. In this case, the ground state of the system does not share the same robustness against noise as in the case of the entanglement protocol. To circumvent this problem, we propose the inclusion of a local control field that can drive the system to an intermediate state, which is more robust against noise in comparison to other states. The target state is also achieved by a fast pulse close to the final time. We find that this approach provides a significant gain and promises to improve the realization of quantum computing in the so-called noisy intermediate-scale quantum devices.

I. INTRODUCTION

Quantum computing holds the promise of surpassing the performance of its classical counterpart, leading to a new era of technological advances. However, there exist severe bottlenecks to performing quantum computing with full power, the main one concerning the intrinsic noise of the quantum hardware, which constrains the number of qubits that can be used in practice. Nevertheless, quantum hardware with some tens of qubits is accessible and a great amount of effort has been devoted to operating these currently available machines, known as noisy intermediate-scale quantum (NISQ) devices [1].

Among the classes of algorithms that can run on NISQ devices are the adiabatic quantum algorithms, which are based on a combination of time-independent Hamiltonians [2,3]. Through the adiabatic theorem, the Hamiltonian adiabatically switches from the so-called driving Hamiltonian, whose ground state can in principle be easily prepared, to the problem Hamiltonian, whose ground state encodes the solution of the computational task. Adiabatic quantum algorithms use the fact that a quantum system remains in its instantaneous eigenstate given that the evolution is carried out sufficiently slowly (adiabatic theorem) [4]. The drawback of this approach is the required time to keep the adiabatic theorem valid, which can be too long for real applications. Furthermore, the final ground state can be drastically affected because of the action of noise for sufficiently long times. Several alternatives have been proposed to attack this problem, such as the local adiabatic evolution or the use of counterdiabatic drivings [5–10]. Another approach relies on the applications of optimal

control theory (OCT) to adiabatic inspired quantum algorithms [11–15]. In this approach, the framework of the driving and problem Hamiltonians is kept, but the dynamics is no longer adiabatic, meaning that the condition for the adiabatic theorem generally does not hold. This type of quantum computation has been called diabatic quantum annealing, where the time evolution does not necessarily go along with the instantaneous energy eigenstates and diabatic transitions are allowed [8].

Recently, we investigated the problem of finding an unknown target state using OCT for the teleportation protocol built for diabatic quantum annealing, without taking into account dissipative effects [15]. For bounded controls, wherein constraints are imposed on the amplitude of the control functions, we identify an optimal solution, called the double-bang solution, characterized by simply setting both control functions at their maximum values during the entire evolution under certain conditions. We successfully applied this solution to the teleportation protocol considering three qubits, where the goal is to teleport the first qubit to the third qubit [16]. Also, we utilized the Krotov method for open quantum systems to derive optimized controls for manipulating qubit or qutrit systems surrounded by an external environment [17]. Two distinct procedures to obtain the controls were employed: (i) the nonunitary optimization, where the noise is taken into account during the optimization process, and (ii) the unitary optimization, where the optimization is performed for a noise-free system. Subsequently, the resulting controls from unitary optimization were probed considering environmental noise. Both procedures were contrasted, and we found that controls derived from nonunitary optimization demonstrated superior performance compared to those from unitary optimization for state preparation. However, this superiority does not hold for quantum gate implementation in

---

*lkcastelano@df.ufscar.br

scenarios where noise is modeled by the Markovian master equation.

In this paper we apply OCT techniques to diabatic quantum annealing protocols operating in the presence of noise. The controls obtained by OCT can perform the computational task faster than the usual adiabatic quantum computing. Initially, we consider the entanglement protocol designed for two qubits. Intriguingly, our findings reveal the robustness of this protocol against noise, meaning that it is possible to attain the entangled state for arbitrarily high values of the noise strength. The reason behind this fact is related to the chosen Hamiltonians, where the ground state of the driving Hamiltonian is not affected by the noise. The optimized control solution dictates the maintenance of the system in its ground state, followed by the application of a fast pulse to promote the entanglement of the qubits at the end of the time evolution.

Subsequently, we consider the teleportation protocol, where the ground state of the system is not immune to the influence of noise, differing from the case of the entanglement protocol. To enhance the performance of this protocol, we propose the inclusion of an extra control term in the Hamiltonian that can drive the system to an intermediate state, which is less affected by the noise in comparison to other states. As in the entanglement protocol, the desired outcome of the teleportation protocol is realized by a fast pulse at the end of the time evolution. We find that this approach yields a significant reduction in the mean value of the problem Hamiltonian at the end of the protocol, therefore approaching its ground state. The concept of Hamiltonian engineering, aimed at mitigating the impact of noise, has also been applied to nitrogen-vacancy. centers in diamond [18] and in nuclear spins in quantum dots [19] with great success.

II. ENTANGLEMENT PROTOCOL

We start by considering two independent control functions, which are related to two time-independent Hamiltonians: H_1 (driving) and H_2 (problem) [15]. The system is initially prepared in the ground state of H_1, and the desire is to reach the ground state of H_2 at the final time. The system evolves according to the total time-dependent Hamiltonian

$$H(t) = \varepsilon_1(t)H_1 + \varepsilon_2(t)H_2, \tag{1}$$

where $\varepsilon_1(t)$ and $\varepsilon_2(t)$ are the two independent dimensionless control functions.

We analyze the problem of two qubits, initially in a separable state, that should evolve to an entangled state at a given final time. In this case, the driving and the problem Hamiltonians are given by

$$H_1 = \omega_0\big(\sigma_z^{(1)} + \sigma_z^{(2)}\big), \tag{2}$$

$$H_2 = \omega_0\big(\sigma_y^{(1)}\sigma_y^{(2)} - \sigma_z^{(1)}\sigma_z^{(2)}\big), \tag{3}$$

where $\sigma_m^{(j)}$ is the Pauli spin matrix in the m direction acting on the jth qubit, e.g., $\sigma_z^{(1)} = \sigma_z \otimes \mathbb{1}$. Hereafter, we use the system of units where $\hbar = 1$. The ground states of the Hamiltonians H_1 and H_2 are given by

$$|\phi_0\rangle = |11\rangle, \tag{4}$$

$$|\chi_0\rangle = \frac{1}{\sqrt{2}}(|00\rangle + |11\rangle), \tag{5}$$

respectively, where $|\phi_0\rangle$ is the separable initial state and $|\chi_0\rangle$ is the desired entangled state to be reached at the final time of evolution. Both ground states have the same eigenenergy $E_0 = -2\omega_0$. Under unitary dynamics (no decoherence present), the target can be achieved by the adiabatic approach with $\varepsilon_1(t) = 1 - \varepsilon_2(t)$ [15].

The nonunitary dynamics is described by the Markovian master equation for the density matrix $\rho(t)$,

$$\frac{d\rho(t)}{dt} = \mathcal{L}[\rho], \tag{6}$$

where the Liouvillian that corresponds to physical solutions has the Lindblad form given by

$$\mathcal{L}[\rho] = -i[H, \rho] + \frac{1}{2}\sum_j \gamma_j(2L_j\rho L_j^\dagger - L_j^\dagger L_j\rho - \rho L_j^\dagger L_j), \tag{7}$$

where the first term on the right-hand side represents the unitary evolution, while the second term accounts for the dissipative effects. The L_j are the Lindblad operators and γ_j are the corresponding decay rates.

By following the variational control approach for open quantum systems described in Ref. [20], we are led to a set of equations that must be self-consistently solved. First, we have to solve Eq. (6) considering the initial condition $\rho(0) = \rho_0$ for a given initial state $\rho_0 = |\phi_0\rangle\langle\phi_0|$. Also, we have to solve the equation

$$\frac{d\chi(t)}{dt} = \mathcal{L}^\dagger[\chi], \tag{8}$$

where $\mathcal{L}^\dagger$ is the adjoint of the superoperator given in Eq. (7) and the evolution considers the condition $\chi(T) = H_2\rho(T)H_2$ at the final time $t = T$, which is obtained through the solution of Eq. (6). Finally, the controls are updated through the expression

$$\varepsilon_j^{(k)}(t) = \varepsilon_j^{(k-1)}(t) + \mathrm{Im}\left[\mathrm{Tr}\left(\frac{\chi(t)}{\lambda_j}[H_j, \rho(t)]\right)\right] \tag{9}$$

for $j = 1, 2$, where the index k is related to the kth step within the self-consistent method. The λ_j is a chosen constant that is used together with the number of steps of the self-consistent method to supervise the convergence of the controls $\varepsilon_j(t)$. By solving the set of equations (6)–(9) we can numerically find the controls that maximize the total functional, consequently minimizing the mean energy of the problem Hamiltonian $\langle H_2\rangle(T)$. This approach can be applied to all types of problems inspired by the adiabatic quantum computation, where the goal is to obtain the ground state of the problem Hamiltonian at the end of the dynamics. Usually, this procedure works with high accuracy for closed quantum systems and we would like to investigate the role of dissipative effects.

Here we consider two different types of Lindblad operators, related to the dephasing channel and the amplitude-damping channel, which are archetypal noisy channels [21]. For two qubits, the sum in Eq. (7) contains the terms $j = 1, 2$ and the Lindblad operators are either $L_1 = \sigma_z \otimes \mathbb{1}$ and $L_2 = \mathbb{1} \otimes \sigma_z$ (dephasing) or $L_1 = \sigma_- \otimes \mathbb{1}$ and $L_2 = \mathbb{1} \otimes \sigma_-$ (amplitude damping), where $\sigma_- = (\sigma_x - i\sigma_y)/2$. Figure 1 shows the mean value of the problem Hamiltonian $\langle H_2\rangle(T)$ evaluated at the end of the evolution as a function of the decay rate
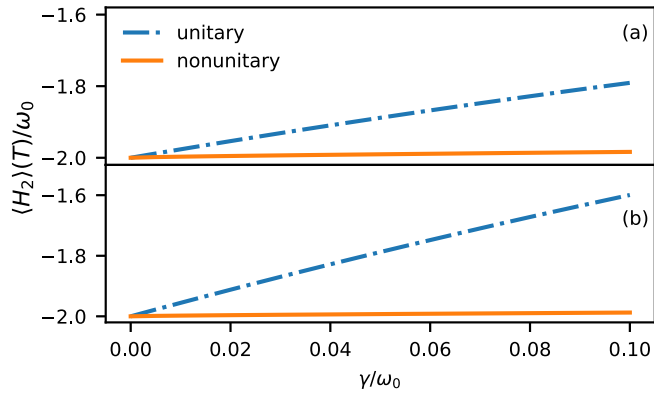
FIG. 1. Mean value of the problem Hamiltonian $\langle H_2 \rangle (T)$ evaluated at the end of the evolution for the entanglement protocol considering (a) dephasing and (b) amplitude-damping errors as a function of the decay rate γ using the control function obtained from the unitary optimization (blue dash-dotted lines) and nonunitary optimization (orange solid lines).

$\gamma_1 = \gamma_2 = \gamma$ for both types of Lindblad operators, the dephasing [Fig. 1(a)] and the amplitude damping [Fig. 1(b)]. It is noteworthy that the mean value has a percent error of less than 1% for the considered range of values of γ when the optimization is evaluated using the nonunitary dynamics (orange solid lines in Fig. 1). In contrast, the results for $\langle H_2 \rangle (T)$ obtained from the unitary optimization diverge from the exact solution as the decay rate increases (blue dotted lines in Fig. 1). In this case, the control fields are obtained for the optimization carried out with $\gamma = 0$, while the mean value $\langle H_2 \rangle (T)$ is evaluated through the time evolution given by Eq. (6) for each different value of γ.

To understand the discrepancy between the unitary and the nonunitary optimization, Fig. 2 shows the optimized controls considering the unitary ($\gamma = 0$) and the nonunitary optimization $\gamma = 0.1\omega_0$, for both dephasing and amplitude-damping types of noise. The fields obtained from the unitary optimization [Fig. 2(a)] are smooth and have a smaller amplitude than the fields obtained from the nonunitary optimization [Figs. 2(b) and 2(c)]. Moreover, the fields resulting from the nonunitary optimization are close to zero in most of the evolution time. Only at the end of the evolution do the control fields behave as strong pulses that can achieve the desired target state. Here it is worth mentioning that a completely equivalent but faster solution would be the application of the same pulses of Figs. 2(b) and 2(c) closer to the initial time.

To further assess the behavior of these controls, Fig. 3 exhibits the population dynamics of the system. Initially, only the state $|\psi_1\rangle = |11\rangle$ is populated. Figure 3(a) presents the dynamics with $\gamma = 0.1\omega_0$ considering the control fields obtained from the unitary optimization. In this case, the population of the state $|00\rangle$ increases, while the population of the state $|11\rangle$ decreases as a function of time. At the final time of evolution, the populations of both states $|00\rangle$ and $|11\rangle$ approach 0.5, but due to the dissipation the desired value cannot be perfectly obtained. Figures 3(b) and 3(c) show the dynamics in the presence of decoherence ($\gamma = 0.1\omega_0$) with the control fields obtained from the nonunitary dynamics. In contrast to Fig. 3(a), the system remains in the initial state
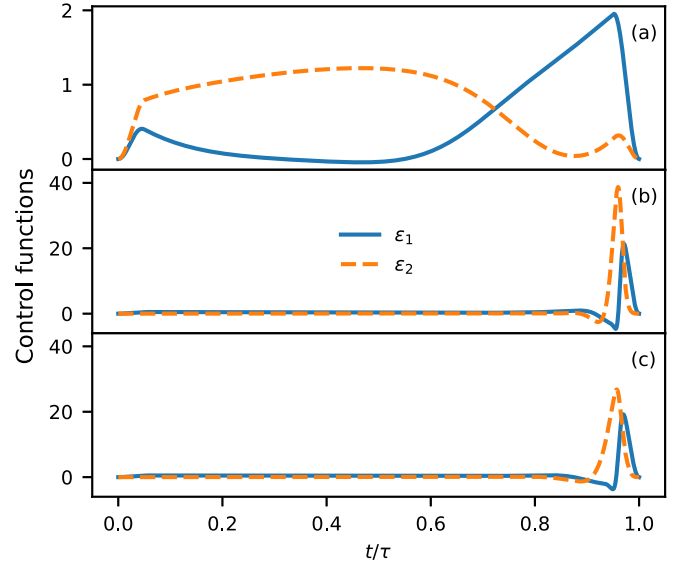

FIG. 2. Optimized control functions ε_1 (blue solid lines) and ε_2 (orange dashed lines) obtained with the objective of minimizing the value of $\langle H_2 \rangle (T)$. (a) Unitary optimization, which does not depend on the type of noise. Also shown are the optimized control functions for a fixed decay rate $\gamma = 0.1\omega_0$ considering the (b) dephasing and (c) amplitude-damping errors.

$|11\rangle$ for as long as possible, while other states are not populated. Only at the end of the time evolution, the state $|00\rangle$ is populated and the target state is reached with very high accuracy at the final time. This result is related to the fact that the nonunitary optimization is searching for optimal control
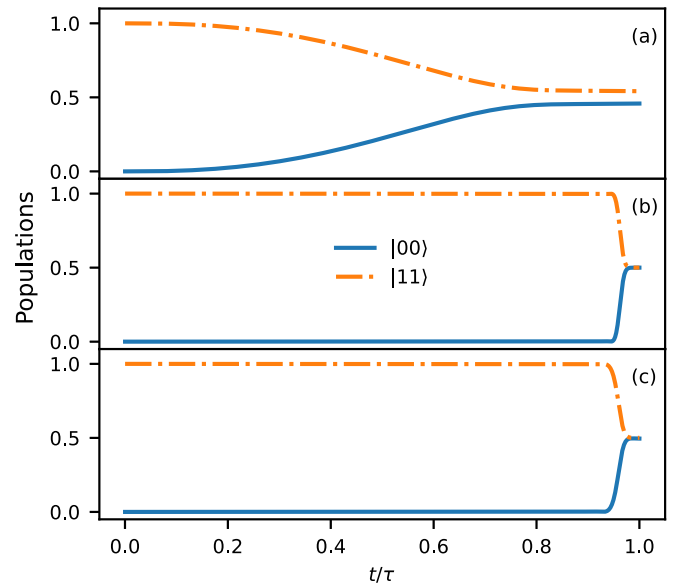

FIG. 3. (a) Population of states as a function of time for the entanglement protocol resulting from the unitary optimization. Also shown is the population of states as a function of time for the entanglement protocol with a fixed decay rate $\gamma = 0.1\omega_0$ resulting from nonunitary optimization for the (b) dephasing and (c) amplitude-damping noises. The population of states $|00\rangle$ and $|11\rangle$ are shown by blue solid and orange dash-dotted lines, respectively.

functions that minimize the effects of noise. One possible way to accomplish such a task is to leave the system in states that are less affected by the dissipation. In the present case, the initial state is free from dissipation. After all, it does not suffer from the spontaneous decay (amplitude-damping noise) or dephasing effects, because it is a separable state. Therefore, in the dissipative case, the optimal controls are such that they leave the system essentially unperturbed up to very close to the final evolution time. Then the controls act with a large amplitude to perform the desired transition in a short time, thus diminishing overall dissipative effects.

III. TELEPORTATION PROTOCOL

As a second instance of the application of OCT to improve algorithms based on the adiabatic quantum computation, we consider the teleportation protocol. In this protocol, there are three qubits whose dynamics are associated with the driving Hamiltonian

$$H_1 = -\omega_0 \left(\sigma_x^{(2)} \sigma_x^{(3)} + \sigma_z^{(2)} \sigma_z^{(3)} \right), \tag{10}$$

for which the ground state is twofold degenerate $|\phi_0^{(1)}\rangle = |0\rangle \otimes |\Phi\rangle$ and $|\phi_0^{(2)}\rangle = |1\rangle \otimes |\Phi\rangle$, where $|\Phi\rangle$ is a Bell state $|\Phi\rangle = (|00\rangle + |11\rangle)/\sqrt{2}$. The problem Hamiltonian is given by

$$H_2 = -\omega_0 \left(\sigma_x^{(1)} \sigma_x^{(2)} + \sigma_z^{(1)} \sigma_z^{(2)} \right), \tag{11}$$

whose ground state is also a twofold-degenerate state with energy $E_0 = -2\omega_0$ given by $|\chi_0^{(1)}\rangle = |\Phi\rangle \otimes |0\rangle$ and $|\chi_0^{(2)}\rangle = |\Phi\rangle \otimes |1\rangle$.

This protocol aims at teleporting the information initially encoded into the first qubit to the third qubit at the final time of evolution, which is equivalent to a SWAP gate. The initial state can be chosen as any linear combination of states $|\chi_0^1\rangle$ and $|\chi_0^2\rangle$ without loss of generality [16]. In this particular case, the initial state is a linear combination of entangled states that are tricky to initially prepare without error [22]. Therefore, we are assuming that these states are perfectly prepared, which differs from the current state of art. This type of error would lead to a reduction in the performance of the optimization procedure depending on the magnitude of the initialization error. Interestingly, there are some advances in this direction using OCT, but this approach is beyond the scope of the present work [23,24].

As already discussed in Ref. [16], one-qubit gates can be obtained by the unitary transformation of the driving Hamiltonian $H_1' = U_G H_1 U_G^\dagger$, where U_G is the one-qubit gate acting on the third qubit, which can be obtained by local magnetic fields (the same idea can be generalized to implement two-qubit gates; see [16] for more details). To describe dissipative effects, we choose independent Lindblad operators given by $L_i = s^{(i)}$, where $i = 1, 2$, and 3 is the index related to the qubit that the operator is acting on it, e.g., the Lindblad operator acting on the first qubit is $L_1 = s \otimes \mathbb{1} \otimes \mathbb{1}$, where $s = \sigma_- = |1\rangle\langle 0|$ for amplitude damping and $s = \sigma_z$ for dephasing.

The mean values $\langle H_2 \rangle(T)$, resulting from application of the OCT to the teleportation protocol, for the nonunitary and the unitary optimization for both dephasing and amplitude damping as a function of the decay rate are shown in Fig. 4.
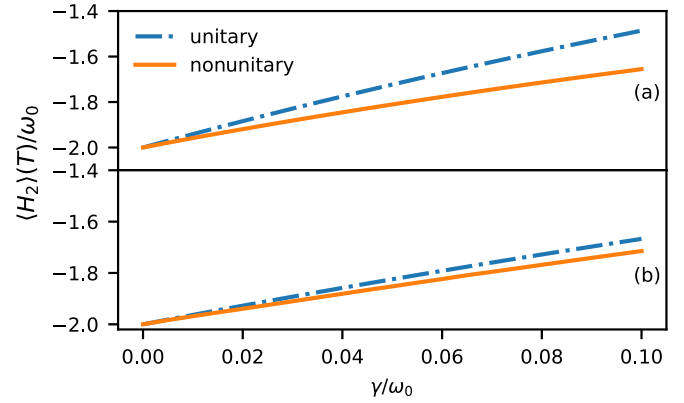

FIG. 4. Mean value of the problem Hamiltonian $\langle H_2 \rangle(T)$ evaluated at the end of the evolution for the teleportation protocol considering (a) dephasing and (b) amplitude-damping errors as a function of the decay rate γ. The mean value of $\langle H_2 \rangle(T)$ evaluated for two-control Hamiltonians of the type of Eq. (1) obtained from the unitary and nonunitary dynamics is shown by the blue dash-dotted and orange solid lines, respectively.

These results convey the message that the nonunitary optimization does not improve the mean value $\langle H_2 \rangle(T)$ obtained through the unitary optimization by a large factor, as previously found for the entanglement protocol. The respective control functions are shown in Fig. 5 resulting from the unitary optimization [Fig. 5(a)], nonunitary optimization with dephasing [Fig. 5(b)], and nonunitary optimization with amplitude damping [Fig. 5(c)]. For the teleportation protocol, the nonunitary optimization yields control functions that achieve amplitudes that are ten times larger than the amplitude of the
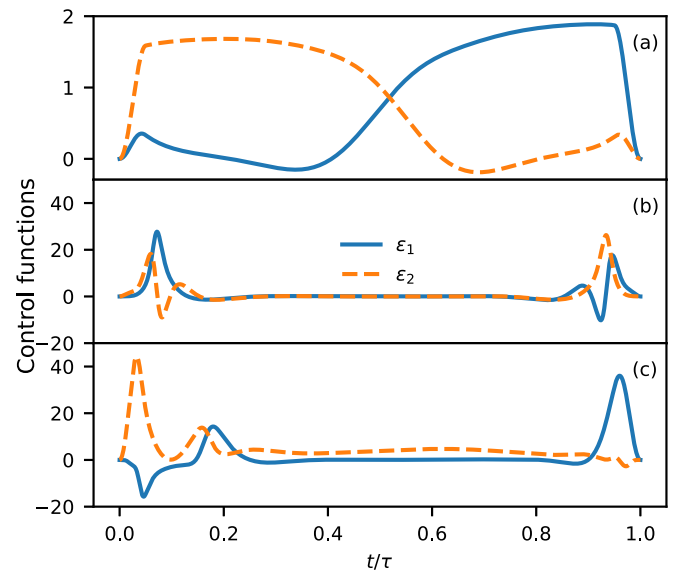

FIG. 5. Optimized two-control functions ε_j obtained for the teleportation protocol using the Hamiltonian described in Eqs. (10) and (11). (a) Unitary optimization ($\gamma = 0$). Also shown are the optimized two-control functions for a fixed decay rate $\gamma = 0.1\omega_0$ considering the (b) dephasing and (c) amplitude-damping errors. The orange dashed lines correspond to $\varepsilon_1(t)$ and the blue solid lines correspond to $\varepsilon_2(t)$.
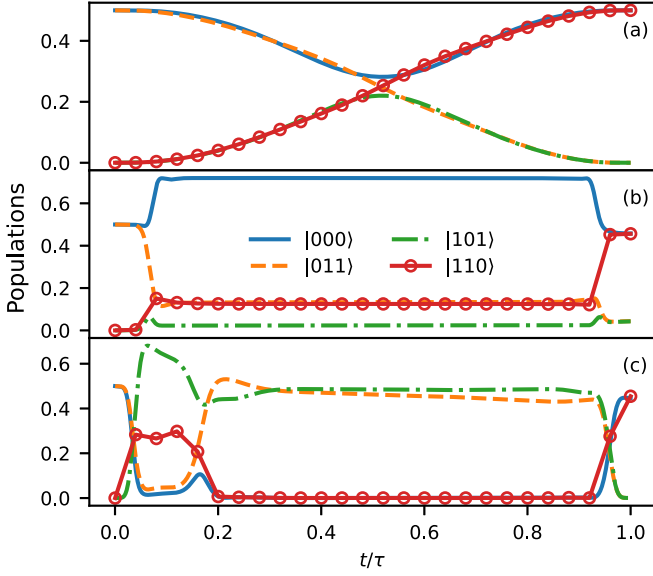
FIG. 6. (a) Population of states as a function of time for the teleportation protocol considering two-control functions, resulting from the unitary optimization. Also shown is the population of states as a function of time for the teleportation protocol with a fixed decay rate $\gamma = 0.1\omega_0$ resulting from the nonunitary optimization for the (b) dephasing and (c) amplitude-damping noises. The populations of states $|000\rangle$ and $|011\rangle$ are given by blue solid lines and orange dash-dotted lines, respectively, and the populations of states $|101\rangle$ and $|110\rangle$ are specified by green dash-dotted lines and red solid lines with open circles.

unitary optimized control fields. Also, the nonunitary control fields are given by pulses at the beginning and at the end of the dynamics, in contrast to the always-on form of the control fields obtained in the unitary optimization. Figure 6 shows the population dynamics corresponding to the control functions of Fig. 5. We use one of the twofold-degenerate ground states of the Hamiltonian H_1 as the initial state, which is given by $|\psi(0)\rangle = \frac{1}{\sqrt{2}}|0\rangle \otimes (|00\rangle + |11\rangle)$, while the corresponding teleported state is $|\psi(T)\rangle = \frac{1}{\sqrt{2}}(|00\rangle + |11\rangle) \otimes |0\rangle$. In the absence of noise and with the unitary-optimized control functions, the occupation of the state $|011\rangle$ smoothly decreases while increasing the amplitude of the state $|110\rangle$; also the state $|101\rangle$ is populated during the dynamics [Fig. 6(a)]. In the presence of the dephasing noise and with the nonunitary-optimized control functions, the occupation of the states $|000\rangle$ and $|110\rangle$ rapidly increases while decreasing the population of the state $|011\rangle$. The populations of those three states are kept almost constant during the dynamics until the final pulselike portion of the controls starts to act, as shown in Fig. 5(b). In this case, the occupation of the states $|000\rangle$ and $|011\rangle$ rapidly decreases and the population of the state $|110\rangle$ increases to reach the target state. A similar behavior happens for the amplitude-damping type of noise, as can be observed in Fig. 5(c). Although the unitary and nonunitary optimizations use different pathways to achieve the lowest mean value $\langle H_2\rangle(T)$, the net effect found for the teleportation protocol is small, in contrast to the entanglement protocol case. This result can be justified by the fact that the nonunitary

TABLE I. Mean value of the problem Hamiltonian $\langle H_2\rangle(T)$ for different types of local fields H_3 included in the Hamiltonian of Eq. (12).

H_3	Dephasing	Amplitude damping
$\sigma_x^{(1)}$	$-1.911\omega_0$	$-1.752\omega_0$
$\sigma_x^{(2)}$	$-1.653\omega_0$	$-1.780\omega_0$
$\sigma_x^{(3)}$	$-1.905\omega_0$	$-1.821\omega_0$
$\sigma_y^{(1)}$	$-1.655\omega_0$	$-1.730\omega_0$
$\sigma_y^{(2)}$	$-1.655\omega_0$	$-1.730\omega_0$
$\sigma_y^{(3)}$	$-1.655\omega_0$	$-1.730\omega_0$
$\sigma_z^{(1)}$	$-1.953\omega_0$	$-1.959\omega_0$
$\sigma_z^{(2)}$	$-1.653\omega_0$	$-1.935\omega_0$
$\sigma_z^{(3)}$	$-1.933\omega_0$	$-1.950\omega_0$

optimization cannot avoid the effects of noise due to the symmetry of the proposed Hamiltonian.

This last result suggests that some improvement may be achieved by changing the structure of the system, for instance, by adding an extra term in the Hamiltonian. For the teleportation protocol, we propose a new Hamiltonian given by

$$H = \varepsilon_1(t)H_1 + \varepsilon_2(t)H_2 + \varepsilon_3(t)H_3, \qquad (12)$$

where the extra Hamiltonian is chosen as a local field $H_3 = \sigma_m^{(k)}$ with $m = x$, y, or z and $k = 1$, 2, or 3. This extra term must be added to the self-consistent method; therefore $j = 1$, 2, and 3 in Eqs. (6)–(9). We have tested all combinations of local fields and obtained the results presented in Table I, which shows $\langle H_2\rangle(T)$ for each type of H_3 for both dephasing and amplitude-damping noise considering $\gamma = 0.1\omega_0$. The local field that produces the smallest mean value for the problem Hamiltonian is $H_3 = \sigma_z^{(1)}$ for both dephasing and amplitude damping.

Figure 7 shows the mean value $\langle H_2\rangle(T)$ as a function of the decay rate for the amplitude-damping and dephasing types of noise considering the extra Hamiltonian. One can see
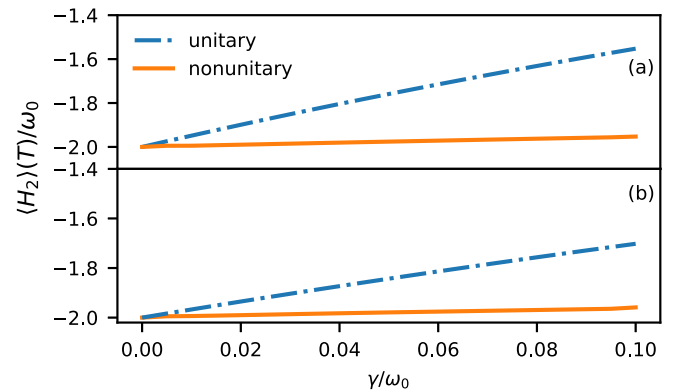

FIG. 7. Mean value of the problem Hamiltonian $\langle H_2\rangle(T)$ evaluated at the end of the evolution for the teleportation protocol considering (a) dephasing and (b) amplitude-damping errors as a function of the decay rate γ. Here the optimized control functions were obtained considering $H_3 = \sigma_z^{(1)}$ in the Hamiltonian of Eq. (12). The unitary and nonunitary optimizations are shown by the blue dash-dotted and orange solid lines, respectively.
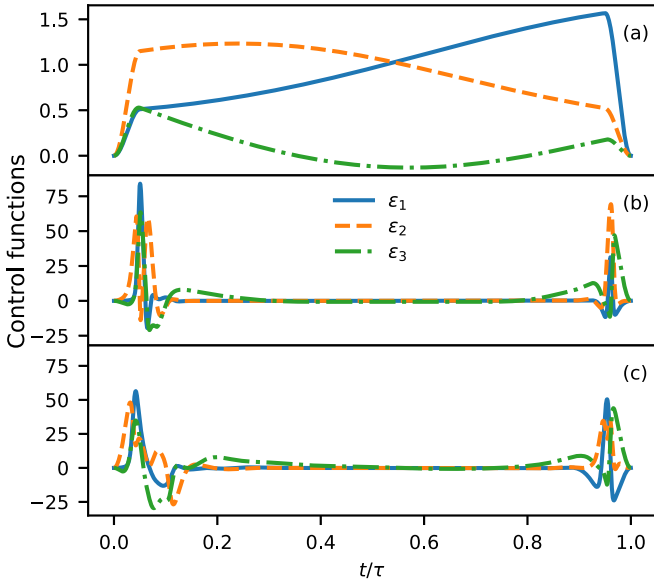
FIG. 8. Optimized three-control functions ε_j obtained for the teleportation protocol using $H_3 = \sigma_z^{(1)}$ in the Hamiltonian of Eq. (12). (a) Unitary optimization ($\gamma = 0$). Also shown are the optimized three-control functions for a fixed decay rate $\gamma = 0.1\omega_0$ considering the (b) dephasing and (c) amplitude-damping errors. The blue solid lines correspond to $\varepsilon_1(t)$, the orange dashed lines correspond to $\varepsilon_2(t)$, and the green dash-dotted lines correspond to $\varepsilon_3(t)$.

that the mean value $\langle H_2 \rangle(T)$ evaluated with the control fields obtained from the nonunitary optimization is smaller than the one calculated from the unitary optimization. For $\gamma = 0.1\omega_0$, $\langle H_2 \rangle(T) = -1.95\omega_0$ for the nonunitary optimization, which is very close to the minimum value of $-2\omega_0$, while the mean value $\langle H_2 \rangle(T) = -1.7\omega_0$ for the unitary optimization, when three Hamiltonians are taken into account. This result can be understood through the analysis of the control fields and population dynamics. The OCT finds controls that have pulses at the beginning and at the end of the time evolution as optimal solutions for both cases, the dephasing [Fig. 8(a)] and the amplitude-damping [Fig. 8(b)] types of noise. For the unitary optimization, the control functions drive the initial state $|\psi(0)\rangle = \frac{1}{\sqrt{2}}|0\rangle \otimes (|00\rangle + |11\rangle)$ to a linear combination of the states $|000\rangle$, $|011\rangle$, $|101\rangle$, and $|110\rangle$, as shown in Fig. 9(a). In contrast, for the nonunitary optimization, the pulses promote a fast transition from the initial state $|\psi(0)\rangle = \frac{1}{\sqrt{2}}|0\rangle \otimes (|00\rangle + |11\rangle)$ to the intermediate state $|\psi_I\rangle = |110\rangle$, as shown in Figs. 9(b) and 9(c). In this case, only the third qubit is affected by the amplitude-damping noise, which drastically reduces the error caused by the noise. At the end of the time evolution, the pulses transform the intermediate state into the teleported state.

Such results show that an appropriate inclusion of an extra local Hamiltonian can improve the efficiency of the optimization because different pathways can be accessed. As proof of the robustness of the inclusion of the extra Hamiltonian approach, we evaluate the average of the mean value of the problem Hamiltonian $\langle H_2 \rangle(T)$ considering a myriad of different states that must be teleported from the first to the third
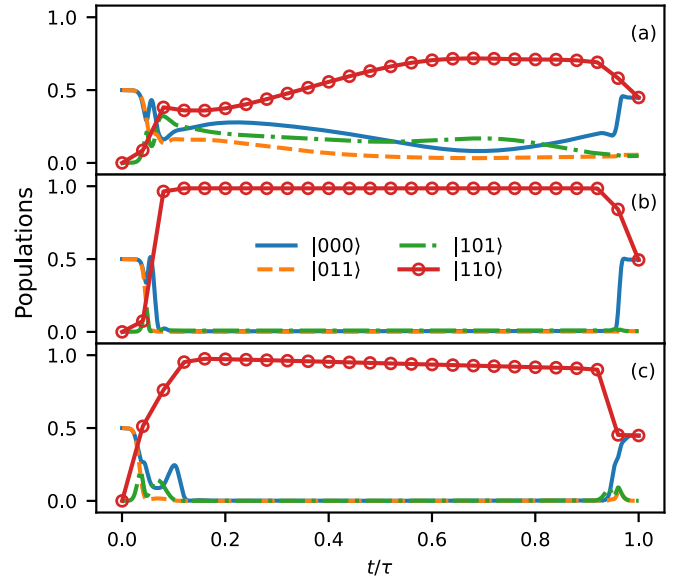

FIG. 9. (a) Population of states as a function of time for the teleportation protocol considering three-control functions resulting from the unitary optimization. Also shown is the population of states as a function of time for the teleportation protocol with a fixed decay rate $\gamma = 0.1\omega_0$ resulting from the nonunitary optimization for (b) dephasing and (c) amplitude-damping noises. The populations of states $|000\rangle$ and $|011\rangle$ are given by blue solid lines and orange dash-dotted lines, respectively, and the populations of states $|101\rangle$ and $|110\rangle$ are specified by green dash-dotted lines and red solid lines with open circles.

qubit. This average is evaluated according to the formula

$$\overline{\langle H_2 \rangle} = \frac{1}{N} \sum_{i=1}^{N} \text{Tr}[\rho_i(T) H_2], \qquad (13)$$

where $\rho_i(T)$ is the solution of Eq. (6) considering the initial state $\rho_i(0) = |\psi_i\rangle\langle\psi_i|$, where $|\psi_i\rangle = (\alpha_i|0\rangle + \beta_i|1\rangle) \otimes |\Phi\rangle$ is a particular initial state from a set of N states. The complex numbers α_i and β_i are random numbers generated through the normal distribution and this procedure produces a proper random pure state [25,26] (see the Appendix for details). In Fig. 10 we plot the average of the mean value of the problem Hamiltonian as a function of the decay rate for $N = 12^4$ states, considering the optimized fields previously found for the initial state $|\psi(0)\rangle = \frac{1}{2}(|0\rangle + |1\rangle) \otimes (|00\rangle + |11\rangle)$. The averages of the mean values of the problem Hamiltonians denoted by $\overline{\langle H_2 \rangle}_3$ and $\overline{\langle H_2 \rangle}_2$ are evaluated considering the total Hamiltonian with or without the extra term, respectively. One can see that the mean value for H_2 evaluated considering the extra term $\overline{\langle H_2 \rangle}_3$ has a much better performance than $\overline{\langle H_2 \rangle}_2$. For example, $\overline{\langle H_2 \rangle}_3 = -1.95\omega_0$ and $\overline{\langle H_2 \rangle}_2 = -1.65\omega_0$ for dephasing and $\overline{\langle H_2 \rangle}_3 = -1.96\omega_0$ and $\overline{\langle H_2 \rangle}_2 = -1.71\omega_0$ for amplitude damping, when $\gamma = 0.1\omega_0$.

In Figs. 8(b) and 8(c) one can notice that the optimized control functions behave as short pulses with high amplitude. This characteristic can be challenging to implement experimentally; therefore, we investigate the role of limiting the amplitude of the control functions. To perform such a task, we include a condition for the amplitudes of the control functions to be bounded in the interval $[-\varepsilon_b, \varepsilon_b]$ by enforcing
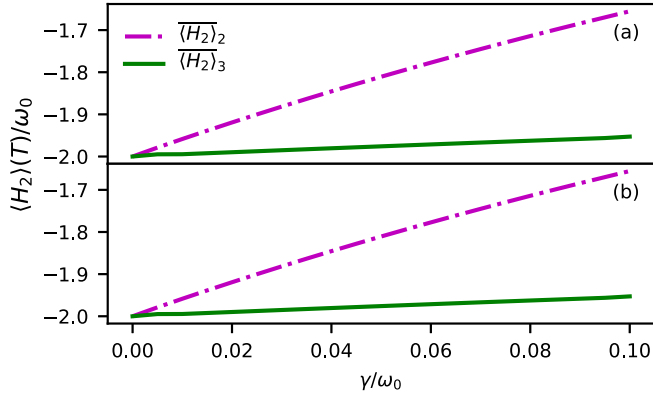
FIG. 10. Average mean value of $\langle H_2 \rangle(T)$, evaluated from Eq. (13) considering $N = 12^4$ random initial states, as a function of the decay rate γ. These random states are built in such a way as to uniformly cover the Bloch sphere relative to the first qubit. Results are plotted for (a) dephasing and (b) amplitude-damping types of error considering the average of the mean values $\overline{\langle H_2 \rangle}_3$ (green solid lines) and $\overline{\langle H_2 \rangle}_2$ (magenta dash-dotted lines) evaluated for three- and two-control functions.

the value of the corresponding limit whenever the controls transcend the bounds. In this case, if the control function $\varepsilon_j(t)$ for $j = 1$, 2, and 3 exceeds one of the bounds $-\varepsilon_b$ or ε_b in a certain time interval, its value is set equal to the crossed bound in this same time interval during the whole self-consistent calculation. In Fig. 11 we plot the control functions considering $\varepsilon_b = 10$ for both dephasing [Fig. 11(a)] and amplitude damping [Fig. 11(b)], when $\gamma = 0.1\omega_0$. One can see in Fig. 11 that the control functions are also pulses limited to $\varepsilon_b = 10$ extended for a larger window of time. This result is in agreement with the area theorem [27] that claims that the area of the pulse must be constant to perform
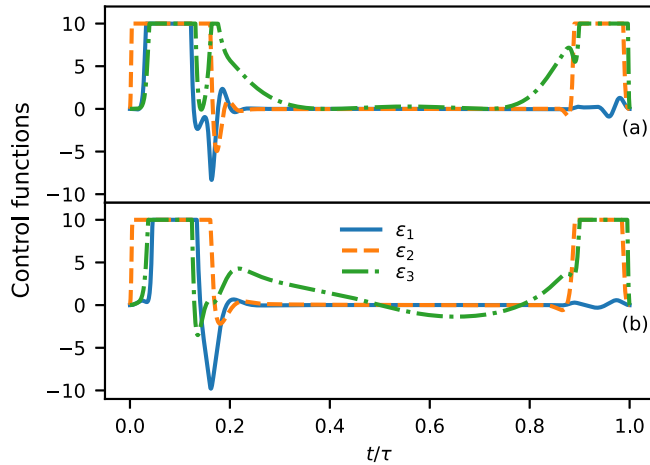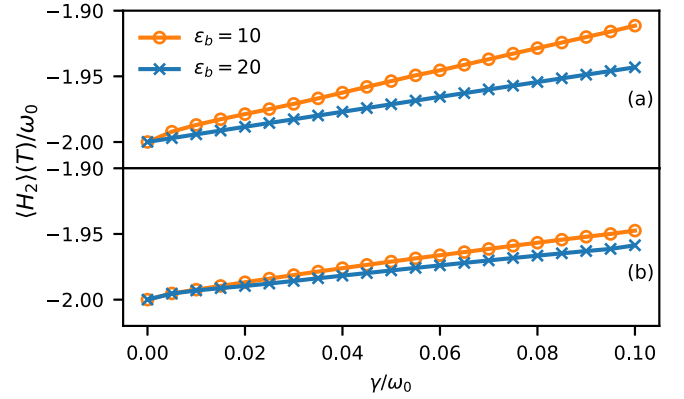

FIG. 12. Mean value of the problem Hamiltonian $\langle H_2 \rangle(T)$ evaluated at the end of the evolution for the teleportation protocol considering (a) dephasing and (b) amplitude-damping errors as a function of the decay rate γ. Here the results are obtained using control functions that are bounded within $[-\varepsilon_b, \varepsilon_b]$, where $\varepsilon_b = 10$ (orange solid lines with open circles) and $\varepsilon_b = 20$ (blue solid lines with crosses).

the transition between the states. In Fig. 12 the mean value $\langle H_2 \rangle(T)$ is shown as a function of the decay rate for two different bound values $\varepsilon_b = 10$ and 20. These results show that the performance of the minimization of $\langle H_2 \rangle(T)$ is not drastically affected by imposing the limits on the amplitude of the control functions. For example, $\langle H_2 \rangle(T) = -1.91\omega_0$ is the worst scenario for $\gamma = 0.1\omega_0$, where $\varepsilon_b = 10$ for dephasing. In comparison to the results without the limiting condition of Fig. 7(a), we have $\langle H_2 \rangle(T) = -1.95\omega_0$ for $\gamma = 0.1\omega_0$ and for an amplitude of the control functions that can be seven times larger than $\varepsilon_b = 10$ [see Fig. 8(b)].

Another aspect that is related to the area theorem concerns the time duration of the control functions. In Fig. 13 we show
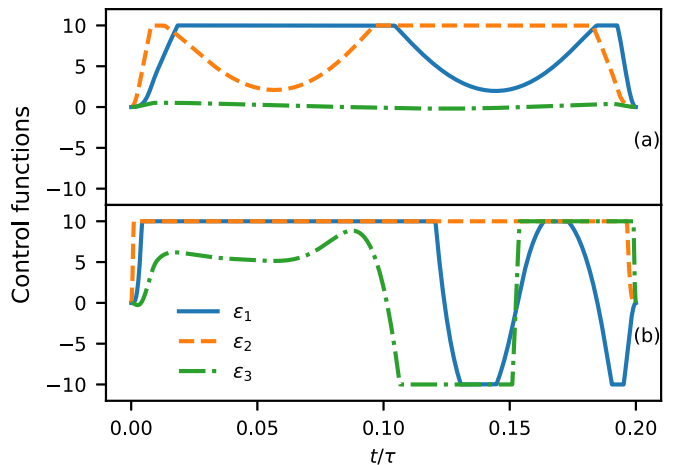

FIG. 11. Optimized three-control functions ε_j obtained for the teleportation protocol using $H_3 = \sigma_z^{(1)}$ in the Hamiltonian of Eq. (12), considering the controls bounded in the interval $[-\varepsilon_b, \varepsilon_b]$, where $\varepsilon_b = 10$. The optimized three-control functions are plotted for a fixed decay rate $\gamma = 0.1\omega_0$ considering the (a) dephasing and (b) amplitude-damping errors. The blue solid lines correspond to $\varepsilon_1(t)$, the orange dashed lines correspond to $\varepsilon_2(t)$, and the green dash-dotted lines correspond to $\varepsilon_3(t)$.

FIG. 13. Optimized three-control functions ε_i obtained for the teleportation protocol using $H_3 = \sigma_z^{(1)}$ in the Hamiltonian of Eq. (12) considering a time evolution up to $T = 0.2\tau$ and $\varepsilon_b = 10$. The optimized three-control functions are plotted for a fixed decay rate $\gamma = 0.1\omega_0$ considering the (a) dephasing and (b) amplitude-damping errors. The blue solid lines correspond to $\varepsilon_1(t)$, the orange dashed lines correspond to $\varepsilon_2(t)$, and the green dash-dotted lines correspond to $\varepsilon_3(t)$.
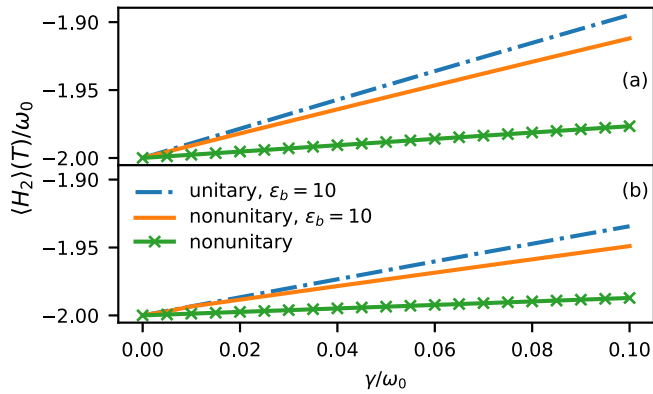
FIG. 14. Mean value of the problem Hamiltonian $\langle H_2 \rangle (T)$ evaluated at the end of the evolution for the teleportation protocol considering (a) dephasing and (b) amplitude-damping errors as a function of the decay rate γ. We consider a time evolution up to $T = 0.2\tau$. Also, the blue dash-dotted and orange solid lines correspond to $\varepsilon_b = 10$ for both unitary and nonunitary optimization, respectively. The green solid lines with crosses correspond to the nonunitary optimization without imposing bounds in the control fields.

the optimized control functions for $\gamma = 0.1\omega_0$ considering $T = 0.2\tau$ and $\varepsilon_b = 10$ for both dephasing [Fig. 13(a)] and amplitude damping [Fig. 13(b)]. According to the area theorem, the short duration of the time evolution implies that the amplitude of the control functions must increase. Thus, the controls no longer behave as two short pulses, except for $\varepsilon_3(t)$ when dephasing noise is considered, as can be observed in Fig. 13.

In Fig. 14 we plot the mean value $\langle H_2 \rangle (T)$ as a function of the decay rate for $T = 0.2\tau$ considering the bound in the amplitude $\varepsilon_b = 10$. We also add the case where no restriction is imposed in the amplitude to check the difference caused by limiting the amplitude. There is still a gain in the performance of the minimization of $\langle H_2 \rangle (T)$ when we compare the unitary and nonunitary optimizations (see Fig. 14). On the other hand, the mean value of $\langle H_2 \rangle (T)$ achieves values closer to the exact value for the nonunitary optimization without limiting the amplitude. For example, the percent errors are 2.5% and 4.5% for the unbounded case and 3.5% and 5.5% for the bounded case for the amplitude-damping and dephasing types of noise, respectively. Although there is a gain for the unbounded case, the maximum amplitude of the control functions can achieve values above 100 (results not shown here), which is ten times larger than the bounded case. This result indicates that the amplitude can be bounded until a certain limit without losing too much information about the ground state of the problem Hamiltonian. Of course, there is a threshold for the reduction of the amplitude. When this threshold is crossed the optimization cannot find the ground state of the problem Hamiltonian even in the absence of noise.

IV. CONCLUSION

In this work we applied OCT for open quantum systems to numerically investigate the performance of algorithms originally proposed for adiabatic quantum computing. We considered two different protocols aimed at performing entan-

glement and teleportation. In the entanglement protocol, we verified that the nonunitary optimization performs much better compared to the unitary optimization. The reason for this improvement is related to the finding of pathways that avoid noise effects. The strategy used by the optimized controls is essentially to leave the system in states that are not affected by the noise, and only close to the end of the time evolution, to act abruptly to drive the system to the desired state, thus spending only a very short time in states that suffer from noise effects. In contrast, the unitary optimization, not impacted by noise effects, drives the system to states more affected by noise, not being capable of avoiding possible errors.

We applied the same analysis for the teleportation protocol. However, in this case, the performance obtained from the nonunitary optimization is similar to that obtained from the unitary optimization. We conjecture that the reason for such comparatively low performance of the nonunitary optimization is related to the type of Hamiltonian used in the teleportation protocol. The proposed Hamiltonian does not allow for pathways that are free from noise effects. To circumvent this problem, we proposed the inclusion of an extra local Hamiltonian. We found that the optimal control function derived by the nonunitary optimization through the inclusion of this extra term performs better in comparison to the unitary optimization. The percent error in finding the ground state of the problem Hamiltonian, considering the average of its mean value, is of order 2.5% for the highest value of decay rate taken into account in our calculations. We also carried out an analysis of the amplitude and duration of the control functions. We found that it is possible to reduce the amplitude of the control functions without losing the performance of the optimization. This result conveys useful information for possible practical implementation, where there is a limit in the real experiments.

In this paper we have not considered other types of errors, such as the measurement and initialization [22] errors. These types of errors play an important role and will affect the performance of the minimization of the energy of the problem Hamiltonian. The former type of error can be mitigated by some techniques based on the reduction of the full assignment matrix [28], while the latter type of error can be dealt with by preparation through steady states [29]. Also, state initialization can benefit from OCT, where robust quantum control can be employed to take care of imperfections [23,24]. We believe that the combination of OCT for open quantum systems with the Hamiltonian engineering in the original protocols can be very interesting in real applications of algorithms related to the diabatic quantum annealing. Since this conclusion has been reached from a limited set of cases, additional investigations have to be carried out to verify its extension to other cases.
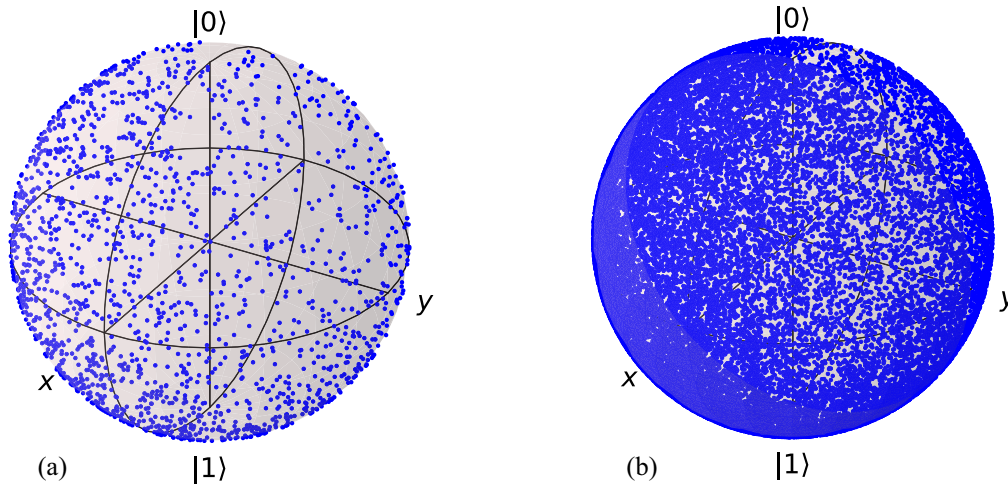
FIG. 15. Random state distribution plotted as points in the Bloch sphere. Blue dots indicate the (a) $N = 12^3$ and (b) $N = 12^4$ random states for a qubit.

APPENDIX: RANDOM STATES FOR QUBITS

For completeness, we provide Fig. 15, which contains points (blue dots) that represent the random states for a qubit plotted in the Bloch sphere using $N = 12^3$ [Fig. 15(a)] and $N_s = 12^4$ points [Fig. 15(b)]. One can see that the sphere is almost completely covered for $N = 12^4$ points, which is the number of points used to calculate the average over the initial random states employed in the calculation of the average of the mean value of the problem Hamiltonian $\overline{\langle H_2 \rangle}$ described in Eq. (13).

[1] J. Preskill, Quantum **2**, 79 (2018).
[2] T. Albash and D. A. Lidar, Rev. Mod. Phys. **90**, 015002 (2018).
[3] R. Barends, A. Shabani, L. Lamata, J. Kelly, A. Mezzacapo, U. L. Heras, R. Babbush, A. G. Fowler, B. Campbell, Y. Chen *et al.*, Nature (London) **534**, 222 (2016).
[4] E. Farhi, J. Goldstone, S. Gutmann, J. Lapan, A. Lundgren, and D. Preda, Science **292**, 472 (2001).
[5] N. N. Hegade, K. Paul, Y. Ding, M. Sanz, F. Albarrán-Arriagada, E. Solano, and X. Chen, Phys. Rev. Appl. **15**, 024038 (2021).
[6] L. Prielinger, A. Hartmann, Y. Yamashiro, K. Nishimura, W. Lechner, and H. Nishimori, Phys. Rev. Res. **3**, 013227 (2021).
[7] A. Callison, M. Festenstein, J. Chen, L. Nita, V. Kendon, and N. Chancellor, PRX Quantum **2**, 010338 (2021).
[8] E. J. Crosson and D. A. Lidar, Nat. Rev. Phys. **3**, 466 (2021).
[9] N. V. Vitanov, A. A. Rangelov, B. W. Shore, and K. Bergmann, Rev. Mod. Phys. **89**, 015006 (2017).
[10] E. Crosson, E. Farhi, C. Y.-Y. Lin, H.-H. Lin, and P. Shor, arXiv:1401.7320.
[11] A. Choquette, A. Di Paolo, P. K. Barkoutsos, D. Sénéchal, I. Tavernelli, and A. Blais, Phys. Rev. Res. **3**, 023092 (2021).
[12] C. Lin, Y. Wang, G. Kolesov, and U. Kalabić, Phys. Rev. A **100**, 022327 (2019).
[13] G. Riviello, K. M. Tibbetts, C. Brif, R. Long, R.-B. Wu, T.-S. Ho, and H. Rabitz, Phys. Rev. A **91**, 043401 (2015).
[14] S. Isermann, Quantum Inf. Process. **20**, 300 (2021).
[15] E. F. de Lima, M. E. F. Fernandes, and L. K. Castelano, Phys. Rev. A **105**, 032454 (2022).
[16] D. Bacon and S. T. Flammia, Phys. Rev. Lett. **103**, 120504 (2009).
[17] M. E. F. Fernandes, F. F. Fanchini, E. F. de Lima, and L. K. Castelano, J. Phys. A: Math. Theor. **56**, 495303 (2023).
[18] X. Rong, J. Geng, F. Shi, Y. Liu, K. Xu, W. Ma, F. Kong, Z. Jiang, Y. Wu, and J. Du, Nat. Commun. **6**, 8748 (2015).
[19] L. Jing, P. Du, H. Tang, and W. Zhang, Phys. Rev. A **107**, 012601 (2023).
[20] N. Suri, F. C. Binder, B. Muralidharan, and S. Vinjanampathy, Eur. Phys. J.: Spec. Top. **227**, 203 (2018).
[21] K. M. F. Romero and R. L. Franco, Phys. Scr. **86**, 065004 (2012).
[22] S. Kak, Found. Phys. **29**, 267 (1999).
[23] H. Zhang and H. Rabitz, Phys. Rev. A **49**, 2241 (1994).
[24] X. Ge, H. Ding, H. Rabitz, and R.-B. Wu, Phys. Rev. A **101**, 052317 (2020).
[25] K. Zyczkowski and H.-J. Sommers, J. Phys. A: Math. Gen. **34**, 7111 (2001).
[26] H.-J. Sommers and K. Zyczkowski, J. Phys. A: Math. Gen. **37**, 8457 (2004).
[27] L. Allen and J. H. Eberly, *Optical Resonance and Two-Level Atoms* (Dover, New York, 1975).
[28] P. D. Nation, H. Kang, N. Sundaresan, and J. M. Gambetta, PRX Quantum **2**, 040326 (2021).
[29] D. Volya and P. Mishra, IEEE Trans. Quantum Eng. **5**, 3100714 (2024).